1 Results: ΛK^0_S and $\Lambda K^{\pm}$

In the following sections, we present our final results, for which three residual contributors are assumed. Results for the cases of ten residual contributors and no residual correlations may be found in Appendices **??** and **??**, respectively. Furthermore, comparisons of results obtained using different variations of the fit method can be found in Appendix **??**.

For the results shown, unless otherwise noted, the following hold true: All correlation functions were normalized in the range $0.32 < k^* < 0.40$ GeV/c, and fit in the range $0.0 < k^* < 0.30$ GeV/c. For the ΛK^- and $\bar{\Lambda} K^+$ analyses, the region $0.19 < k^* < 0.23$ GeV/c was excluded from the fit to exclude the bump caused by the Ω^- resonance. The non-femtoscopic backgrounds for the ΛK^+ and ΛK^- systems were modeled by a (6^{th}-)order polynomial fit to THERMINATOR simulation, while those for the ΛK^0_S were fit with a simple linear form. All analyses were fit simultaneously across all centralities, with a single radius and normalization λ parameter for each centrality bin. Scattering parameters ($\Re f_0$, $\Im f_0$, d_0) were shared between pair-conjugate systems, but assumed unique between the different ΛK charge combinations (i.e. a parameter set describing the ΛK^+ & $\bar{\Lambda} K^-$ system, a second set describing the ΛK^- & $\bar{\Lambda} K^+$ system, and a third for the ΛK^0_S & $\bar{\Lambda} K^0_S$ system). Each correlation function received a unique normalization parameter. The fits were corrected for finite momentum resolution effects, non-femtoscopic backgrounds, and residual correlations resulting from the feed-down from resonances.

Lines and boxes on the experimental data represent statistical and systematic errors, respectively. In the figures showing experimental correlation functions with fits, the black solid curve represents the primary (ΛK) correlation's contribution to the fit. The green line shows the fit to the non-flat background. The purple points show the fit after all residual contributions have been included, and momentum resolution and non-flat background corrections have been applied. The extracted fit values with uncertainties are printed as (fit value) $\pm$ (statistical uncertainty) $\pm$ (systematic uncertainty).

Figure 1 nicely collects and summarizes all of our extracted fit parameters. In the summary plot, we show the extracted scattering parameters in the form of a $\Im f_0$ vs $\Re f_0$ plot, which includes the d_0 values to the right side. We also show the λ vs. radius parameters for all three of our studied centrality bins. The extracted fit parameters are also collected in Table 1. Figure 2 presents our extracted fit radii, along with those of other systems previously analyzed by ALICE [**?**], as a function of pair transverse mass (m_{T}).

Centrality	λ	R
0-10%	1.40 $\pm$ 0.63 (stat.) $\pm$ 0.17 (sys.)	6.24 $\pm$ 0.92 (stat.) $\pm$ 0.66 (sys.)
10-30%	0.90 $\pm$ 0.34 (stat.) $\pm$ 0.17 (sys.)	4.41 $\pm$ 0.50 (stat.) $\pm$ 0.39 (sys.)
30-50%	1.00 $\pm$ 0.34 (stat.) $\pm$ 0.22 (sys.)	3.51 $\pm$ 0.44 (stat.) $\pm$ 0.28 (sys.)

System	$\Re f_0$	$\Im f_0$	d_0
ΛK^+ & $\bar{\Lambda} K^-$	-0.49 $\pm$ 0.19 (stat.) $\pm$ 0.12 (sys.)	0.42 $\pm$ 0.22 (stat.) $\pm$ 0.12 (sys.)	-0.55 $\pm$ 2.22 (stat.) $\pm$ 1.76 (sys.)
ΛK^- & $\bar{\Lambda} K^+$	0.19 $\pm$ 0.15 (stat.) $\pm$ 0.08 (sys.)	0.29 $\pm$ 0.17 (stat.) $\pm$ 0.08 (sys.)	-7.80 $\pm$ 6.15 (stat.) $\pm$ 6.10 (sys.)
ΛK^0_S & $\bar{\Lambda} K^0_S$	0.09 $\pm$ 0.15 (stat.) $\pm$ 0.06 (sys.)	0.53 $\pm$ 0.28 (stat.) $\pm$ 0.13 (sys.)	-2.59 $\pm$ 1.47 (stat.) $\pm$ 3.59 (sys.)

Table 1: Fit Results ΛK, with 3 residual correlations included. The fit procedure is as described in the text. The fit is done on the data with only statistical error bars. The errors marked as "stat." are those returned by MINUIT. The errors marked as "sys." are those which result from my systematic analysis (as outlined in Section **??**).

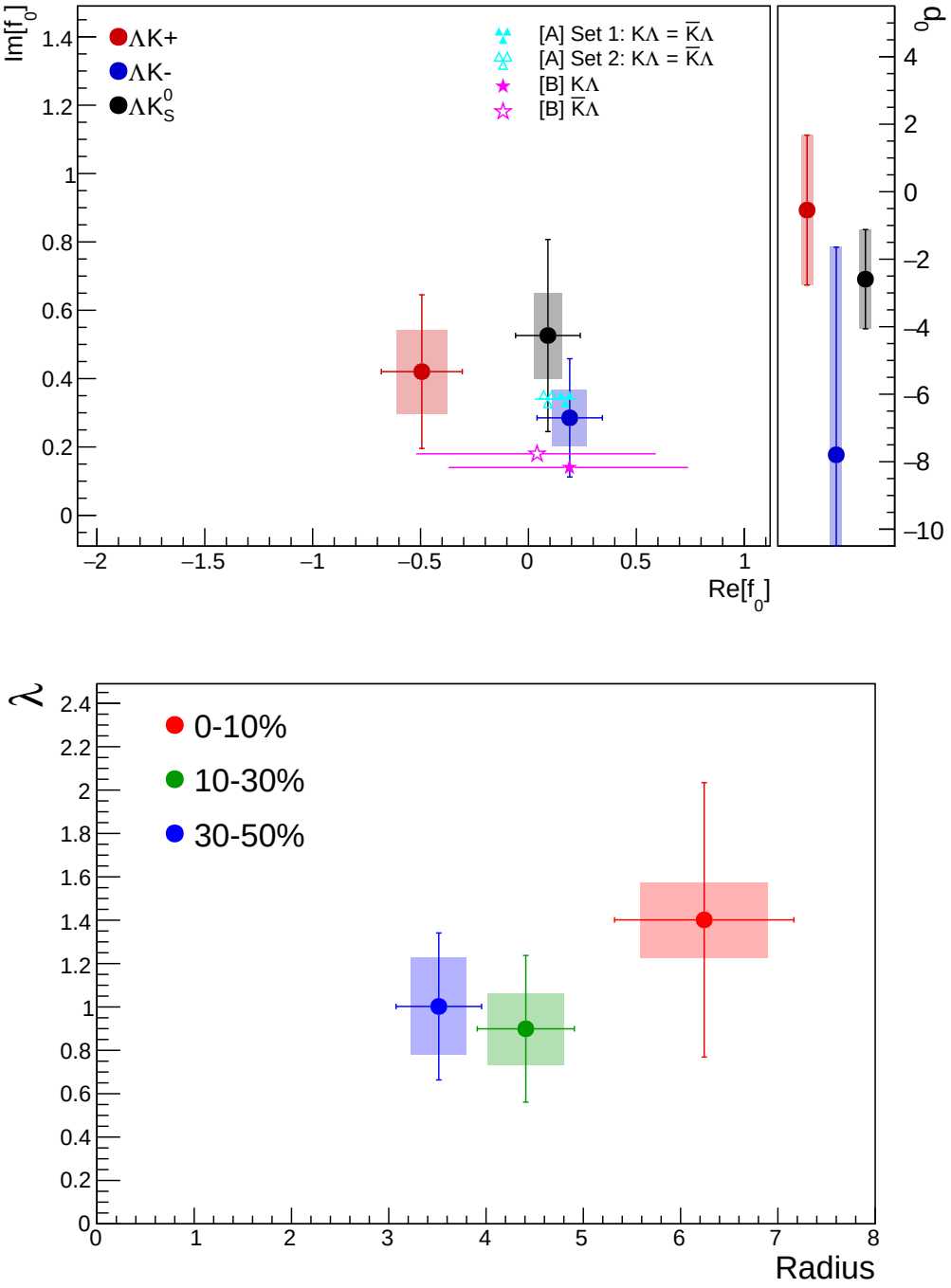

Fig. 1: Extracted fit parameters for the case of 3 residual contributors for all of our ΛK systems. [Top]: $\Im f_0$ vs. $\Re f_0$, together with d_0 to the right. [Bottom]: λ vs. Radius for the 0-10% (blue), 10-30% (green), and 30-50% (red) centrality bins. In the fit, all ΛK systems share common radii. The color scheme used in the panel are to be consistent with those in Fig. 2. The cyan ([A] = Ref. [**?**]) and magenta ([B] = Ref. [**?**]) points show theoretical predictions made using chiral perturbation theory.

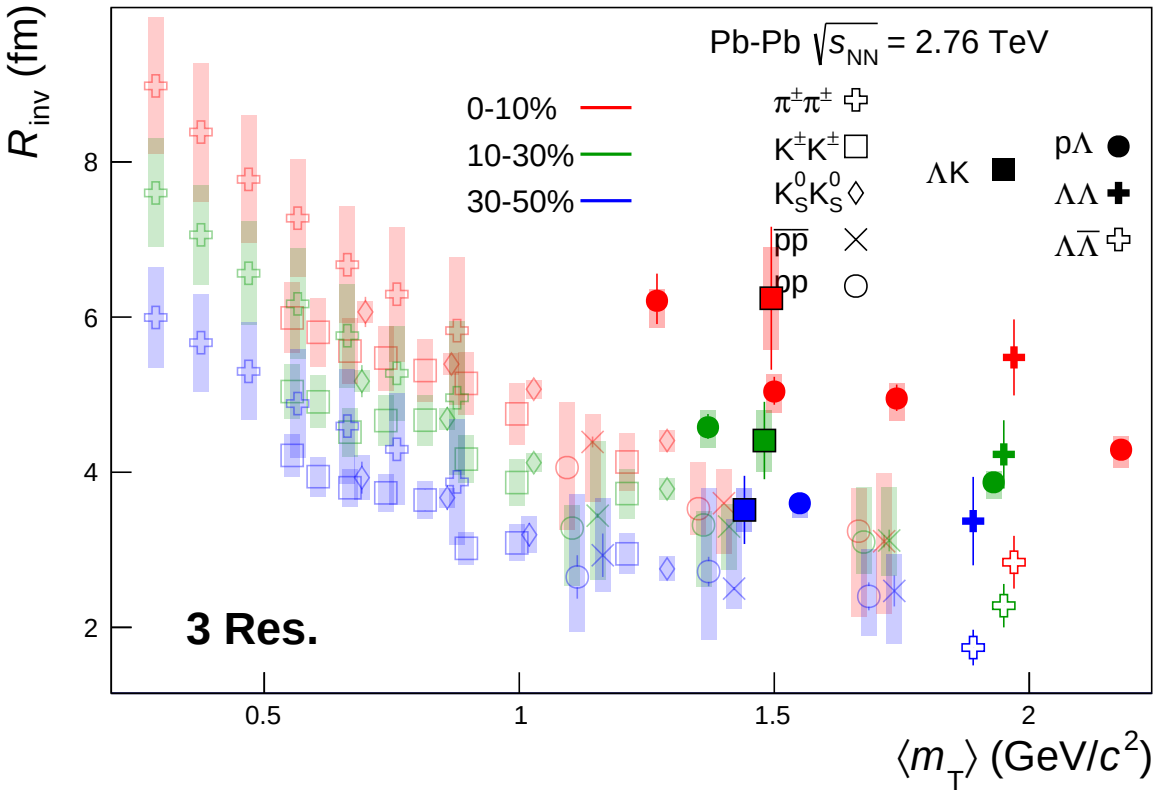

Fig. 2: 3 residual correlations in ΛK fits. Extracted fit $R_{\rm inv}$ parameters as a function of pair transverse mass ($m_{\rm T}$) for various pair systems over several centralities. The ALICE published data [**?**] are shown with transparent, open symbols. The new ΛK results are shown with opaque, filled symbols. The $m_{\rm T}$ value for the ΛK system is an average of those for the ΛK^+, $\bar{\Lambda} K^-$, and ΛK^0_S systems.

1.1 Correlation functions with fits

Figures 3, 4, and 5 show the experimental correlation functions with fits, assuming 3 residual contributors, for all ΛK systems (ΛK^+, ΛK^-, and ΛK^0_S, respectively) in all studied centralities. The parameter sets extracted from the fits can be found in Table 1. Figures with a wider range in k^*, showing better the non-femtoscopic background, may be found in Appendix **??**. Also contained in Appendix **??** are plots demonstrating the contributions from the residuals, as well as results assuming 10 and no residual contributors.

In Figures 3 - 5, the pair system (e.g. ΛK^+) data is shown in the left column, and the conjugate pair system (e.g. $\bar{\Lambda} K^-$) in the right The rows differentiate the different centrality bins (0-10% in the top, 10-30% in the middle, and 30-50% in the bottom). The lines on the data represent the statistical errors, while the boxes represent the systematic errors. The fit procedure is as described in the text; in short, all systems are fit simultaneously with shared radii, while each [ΛK^+, ΛK^-, ΛK^0_S] maintains a unique set of scattering parameters. The black solid line represents the primary ΛK component of the fit. The green line shows the fit to the non-flat background. The purple points show the fit after all residuals' contributions have been included, and momentum resolution and non-flat background corrections have been applied. The extracted fit values with uncertainties are printed in the top left panel of each figure.

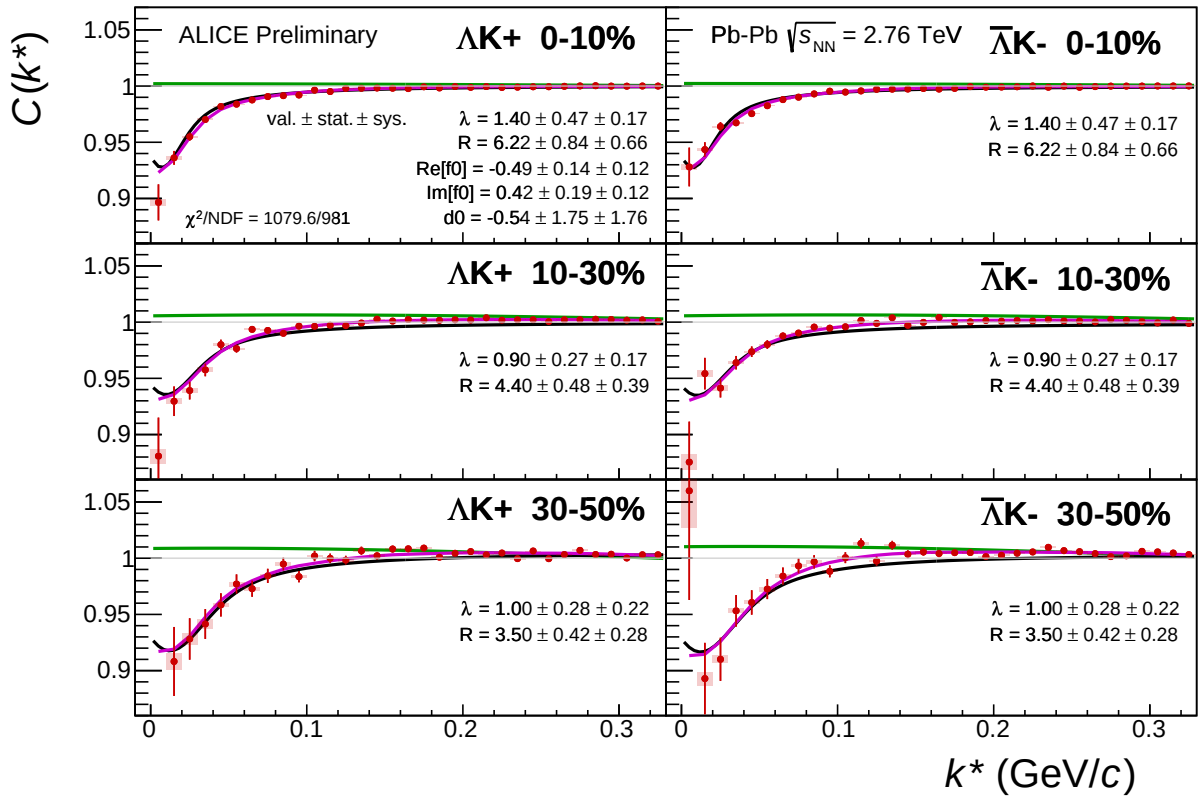

Fig. 3: Fit results, with 3 residual correlations included, for the ΛK^+ and $\bar{\Lambda} K^-$ data. The ΛK^+ data is shown in the left column, the $\bar{\Lambda} K^-$ in the right, and the rows differentiate the different centrality bins (0-10% in the top, 10-30% in the middle, and 30-50% in the bottom). See text for further details.

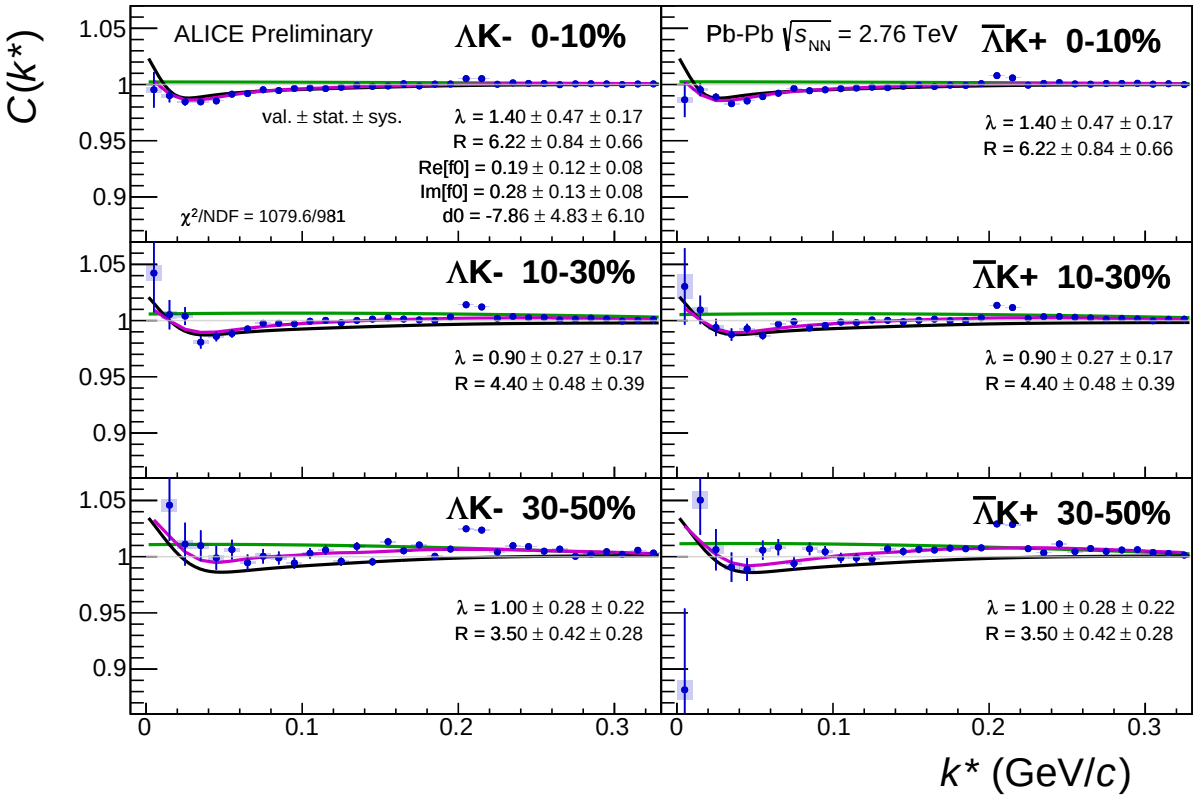

Fig. 4: Fit results, with 3 residual correlations included, for the ΛK^- and $\bar{\Lambda} K^+$ data. The ΛK^- data is shown in the left column, the $\bar{\Lambda} K^+$ in the right, and the rows differentiate the different centrality bins (0-10% in the top, 10-30% in the middle, and 30-50% in the bottom). See text for further details.

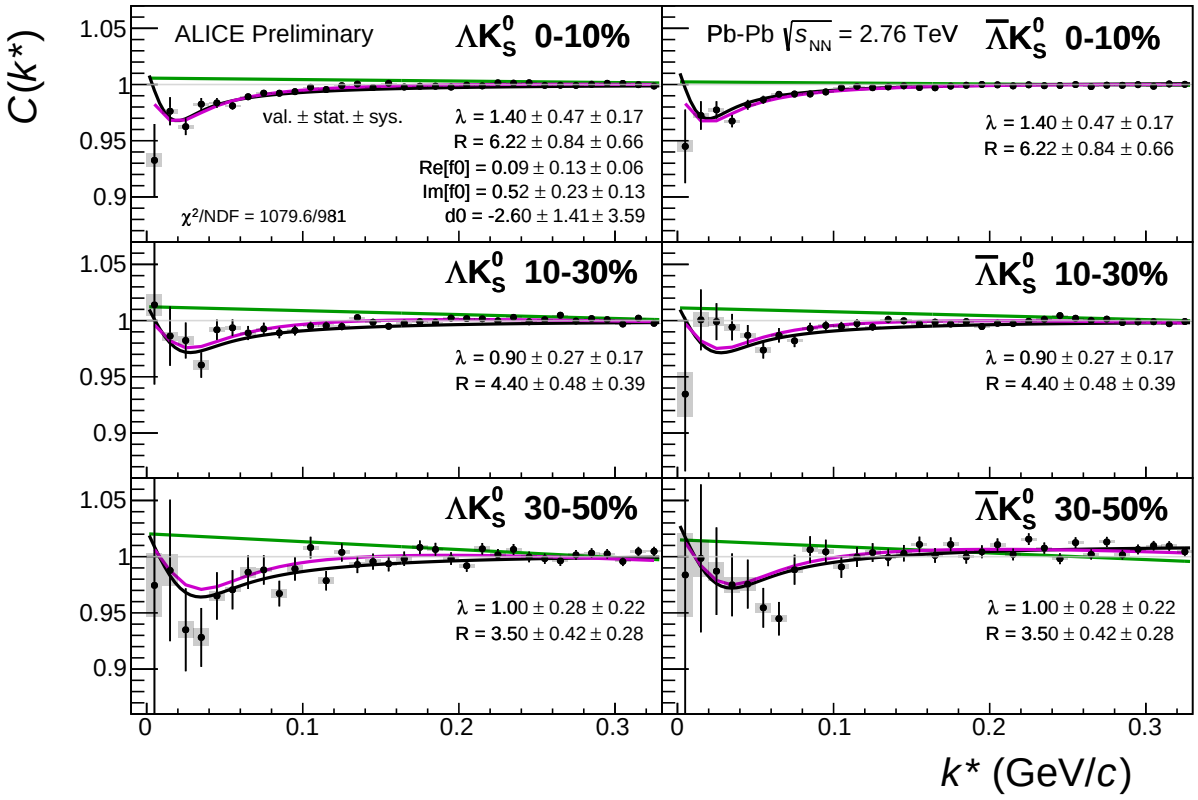

Fig. 5: Fit results, with 3 residual correlations included, for the ΛK^0_S and $\bar{\Lambda} K^0_S$ data. The ΛK^0_S data is shown in the left column, the $\bar{\Lambda} K^0_S$ in the right, and the rows differentiate the different centrality bins (0-10% in the top, 10-30% in the middle, and 30-50% in the bottom). See text for further details.

1.2 Discussion of m_{T}-Scaling

It is clear from the results presented in the previous sections, that the ΛK systems do not conform to the approximate m_{T}-scaling of the pair source sizes. At first thought, this may appear to be a troubling result; the approximate scaling is an observed consequence of the collective behavior of the soft (low-p_{T}) sector of the produced system. The Λ and K particles certainly participate in the collective expansion of the QGP medium, so why do their extracted femtoscopic radii not behave as expected? To get straight to the point: the ΛK systems are comprised on non-identical particles, each with its own and unique single particle source. Each source is, in general, unique in both its overall size, and in its space-time position within the produced medium. The hydrodynamic nature of the medium produces the approximate m_{T}-scaling with respect to these single-particle sources, not the pair sources. The combination of these effects, when probing correlations between non-identical particle pairs, leads to extracted radii falling outside of the (identical particle femtoscopy) m_{T}-scaling trend. Figure 6 (which contains the same data as Fig.2), shows again the R_{inv} vs m_{T} plot, but also highlights (with arrows) the approximate individual $\langle m_{\mathrm{T}} \rangle$ values of the single particle distributions.

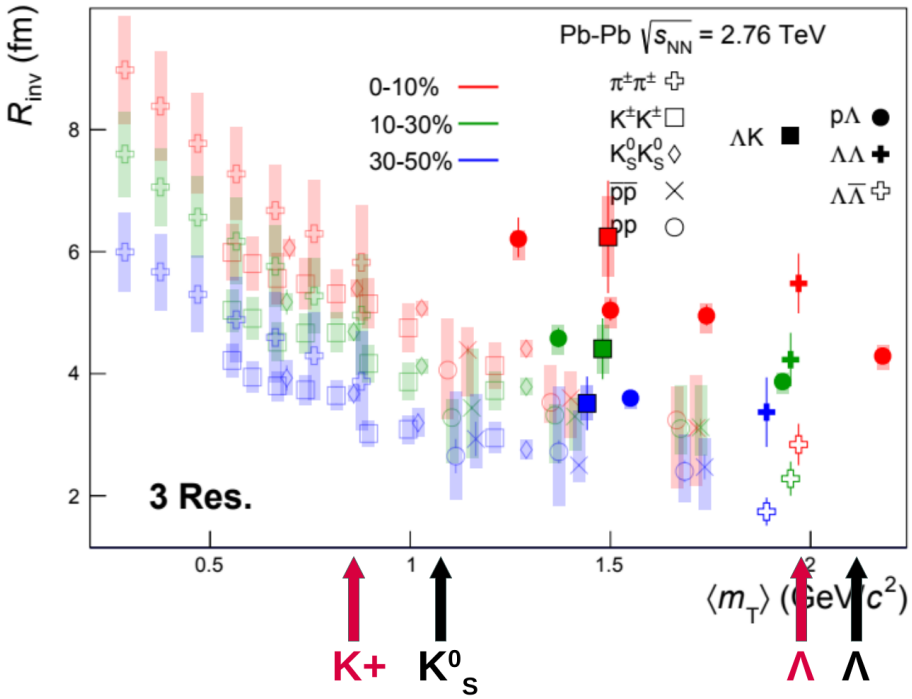

Fig. 6: Same as Fig. 2, but with the individual m_{T} values for the single particle distributions identified. The grey circles show how the single particle sizes are expected to change with m_{T}.

Taking a close look at Fig. 6, one can see that the previously published data (transparent points) are for identical particle analyses only. For these cases, the pair source, probed through femtoscopy, is comprised of two identical sources laying on top of each other. The extracted femtoscopic radii are related to the single particle source sizes by a factor of $\sqrt{2}$, and of course follow the m_{T}-scaling trend. The other (unpublished) non-identical particle femtoscopic study (pΛ) included in the figure, also shows radii deviating from the m_{T}-scaling band. Drawing a comparison with the $\Lambda\bar{\Lambda}$ study shown in Fig. 6 is a bit more complicated; the $\Lambda\bar{\Lambda}$ system, although containing non-identical particles, does contain a particle with its antiparticle, for which annihilation could conceivably alter the pair source distribution. In any case, the pair source m_{T}-scaling visible in the identical particle femtoscopic studies presented in Fig. 6 is really just a manifestation of the scaling of the single particle sources. For the case presented here, sampling single particle distributions with significantly different m_{T} values translates to sampling distributions differing in size which are separated in space-time. Therefore, our results deviating from the m_{T}-scaling curve of the identical particle studies is not surprising.

We can use Fig. 6 to estimate the values of our ΛK radii in the absence of any $\mu_{\rm out}$ offset. As previously stated, for identical particle studies, the single particle radii can be obtained from the extracted femtoscopic radii simply by dividing by $\sqrt{2}$. Using the trends shown in Fig. 6, for the $m_{\rm T}$ values appropriate for our studies, we expect the single particle source sizes in the 0-10% centrality bin to be $R_{\rm K} \sim 5/\sqrt{2}$ fm and $R_{\Lambda} \sim 3/\sqrt{2}$ fm. In Eq. **??** from Sec. **??**, we found the pair source radius was the sum of the single source radii added in quadrature, $R^2_{ab,i} = R^2_{a,i} + R^2_{b,i}$. Therefore, we would expect $R_{\Lambda{\rm K}} \sim 4$ fm, which is clearly below the value we measure. We argue that our larger extracted radii result from a non-zero $\mu_{\rm out}$ in the pair source distribution, due to the fact that the single particle Λ and K sources are separated in space-time. In the following sections, we use simulation (a numerical integration method of the Koonin-Pratt equation, and THERMINATOR 2) to demonstrate the effect on one-dimensional source sizes from non-zero offsets in the "out" direction. Furthermore, we use a spherical harmonic decomposition of our experimental correlation functions to demonstrate that the data are consistent with a non-zero $\mu_{\rm out}$.

We emphasize that we do not suggest our extracted source sizes indicate any sort of contradiction to the hydrodynamic picture of the system dictating the substructure of the femtoscopic radii. In fact, our results rather support such a picture. The hydrodynamic response of the system not only confines higher-$m_{\rm T}$ particles to smaller homogeneity regions, it also pushes their average emissions points further in the "out" direction [**?**]. As introduced above, these effects can lead to larger extracted radii when studying non-identical particle pairs under the assumption of a spherically symmetric Gaussian source with no offset in the "out" direction. This point is further supported with our numerical integration method of the Koonin-Pratt equation (presented below), as well as with our study varying $\mu_{\rm out}$ within the THERMINATOR 2 simulation (presented as the end of this section).

In summary, due to the hydrodynamic response of the system created in heavy-ion collisions, we expect higher-$m_{\rm T}$ particles to originate from smaller regions of homogeneity located further in the "out" direction. This difference in single particle source sizes, in addition to their separation in space-time, can lead to a deviation of non-identical particle studies from the $m_{\rm T}$-scaling trend observed for identical particle pairs. This is not in contradiction to the hydrodynamic response of the system, but rather in support of it. For non-identical particle studies, the individual particle $m_{\rm T}$ values dictate the single particle source sizes and positions, which in turn dictate the observed femtoscopic signal. Therefore, when reporting results from non-identical studies, it is vital to report the individual particle $m_{\rm T}$ values, otherwise, comparisons to other measurements will be impossible.

Numerical integration of the Koonin-Pratt equation

We investigated the effect of a non-zero offset in the outward direction, μ_{out}, by numerically integrating the Koonin-Pratt equation (Eq. **??**), a demonstration of which is shown in Figures 7 and 8. Before going into the details, we find that increasing $\mu_{\rm out}$ leads to a correlation function which is more tightly confined to low-k^* values, i.e. the increase in $\mu_{\rm out}$ makes the source appear larger. The nice analytic form for generating fit correlation functions derived by Lednický relies on a spherically symmetric source distribution centered at the origin. Using instead the method of numerical integration allows us to alter the source as we wish, which, in this case, amounts to simply adding an outward shift, $\mu_{\rm out}$, to the spherically symmetric Gaussian profile. The cost of this flexibility is a significant decrease in the speed of generating fit curves, and this numerical integration is currently too slow to be used within our fit framework. Nonetheless, the numerical integration method does offer a simple test ground for us to study the effect of a non-zero $\mu_{\rm out}$.

For the curves presented in Figs. 7 and 8, a spherically symmetric Gaussian source ($R_o = R_s = R_l$) was assumed, and the offset in the "out" direction ($\mu_{\rm out}$) was varied. In our numerical integration, we used the appropriate forms of the wave-function and scattering parameters (Eqns. **??**-**??**), which were presented in Sec. **??**. In the figure, the closed black circles show the curve generated by our numerical integrator for a radius R_i = 6.24 fm (where i = o, s, l), $\mu_{\rm out}$ = 0 fm, and the parameter sets listed in the

figures ([$\Re f_0, \Im f_0, d_0$] = [-0.49, 0.42, -0.55] for ΛK^+ in Fig. 7, and [$\Re f_0, \Im f_0, d_0$] = [0.19, 0.29, -7.80] for ΛK^- in Fig. 8). Note, the radius of 6.24 fm and the parameter sets were chosen to qualitatively match the ΛK^+ and ΛK^- experimental data. The open magenta circles were generated using the analytic Lednický equation (Eqns. **??**-**??** from Sec. **??**). The figure shows that our numerical integration method is consistent with the Lednický equation. All of the triangle points assume a radius of 5 fm, again with the parameter sets listed in the legends of the figure, and the different colors correspond to different μ_{out} values.

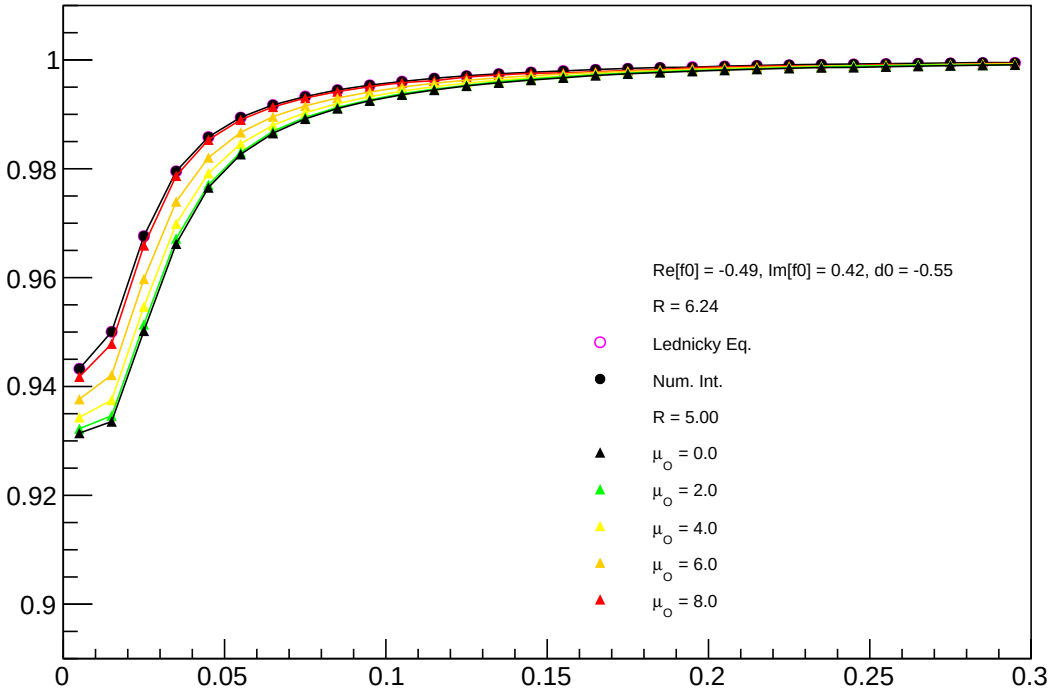

Fig. 7: Numerical integration of the Koonin-Pratt equation, allowing us to study the effect of a non-zero offset in the out direction, μ_{out}. We chose a parameter set to qualitatively match our ΛK^+ data. The assumed scattering parameter set is printed in the top of the legend. All points assume $\mu_{\text{side}} = \mu_{\text{long}} = 0$ fm. The closed black circles and open magenta symbols assume $R_i = 6.24$ fm (where i = o,s,l) and $\mu_{\text{out}} = 0$ fm, while the triangle markers assume $R_i = 5$ fm with varying values of μ_{out}. The open magenta circles were obtained with the Lednický equation, all others were obtained with the numerical integration method. See text for more details.

Figures 7 and 8 nicely demonstrate the effect of increasing the magnitude of the offset. Specifically, the figure shows that increasing μ_{out} makes the correlation function more concentrated towards the low-k^* region, which corresponds to larger radii. Furthermore, for a one-dimensional analysis, we see that the case of a spherically symmetric source with $R_i = 6.24$ fm (where i = o,s,l) is nearly indistinguishable from a source with $R_i = 5$ fm and $\mu_{\text{out}} = 8$ fm. Therefore, even with a fast numerical integrator, it would be difficult to disentangle the effects of a larger source radius from a shift in the "out" direction. In order to pursue this direction, outside input constraining these parameters would be necessary. This could be accomplished, for instance, by fixing the single particle source sizes, and therefore the pair source size, using identical KK and $\Lambda\Lambda$ results.

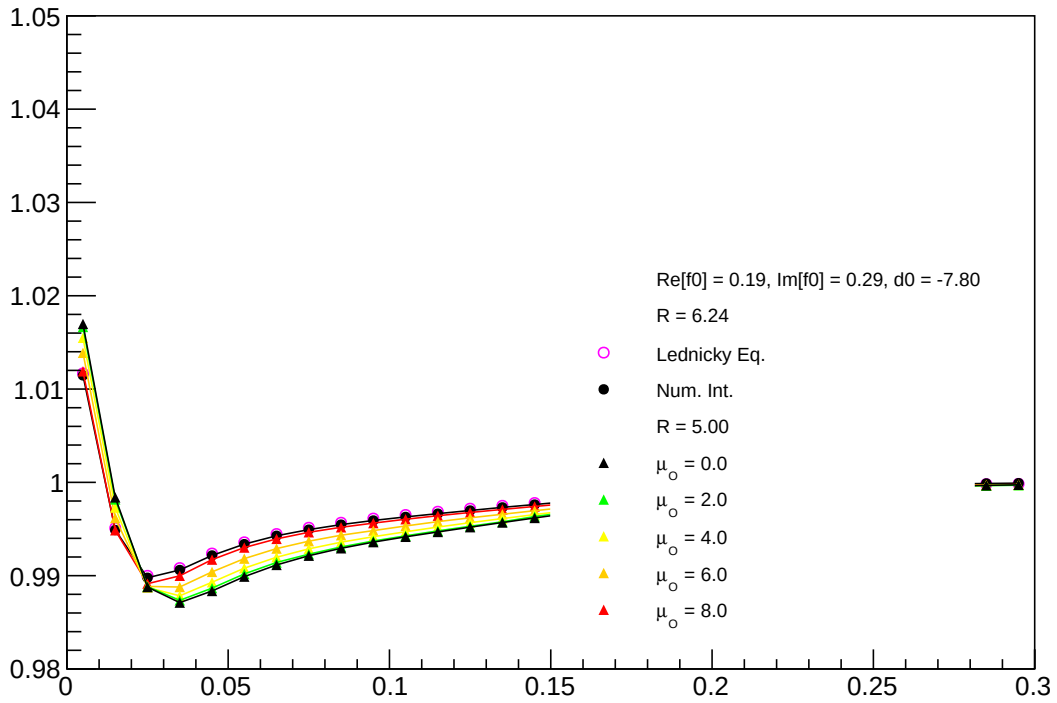

Fig. 8: Numerical integration of the Koonin-Pratt equation, allowing us to study the effect of a non-zero offset in the out direction, μ_{out}. We chose a parameter set to qualitatively match our ΛK^- data. The assumed scattering parameter set is printed in the top of the legend. All points assume $\mu_{\text{side}} = \mu_{\text{long}} = 0$ fm. The closed black circles and open magenta symbols assume $R_i = 6.24$ fm (where i = o,s,l) and $\mu_{\text{out}} = 0$ fm, while the triangle markers assume $R_i = 5$ fm with varying values of μ_{out}. The open magenta circles were obtained with the Lednický equation, all others were obtained with the numerical integration method. See text for more details.

Spherical harmonics and varying μ_{out} with THERMINATOR 2

Identical particle femtoscopic studies are able to probe only the size of the emitting region, or, more precisely, the second moments of the emission function. In addition to this, non-identical particle studies are able to measure the relative emission shifts, the first moments of the emission function. One method to extract information about the emission asymmetries in the system is via a spherical decomposition of the correlation function. With this method, one can draw a wealth of information from just a few components of the decomposition. More specifically, the C_{00} component is similar to the 1D correlation functions typically studied, and probes the overall size of the source. The $\Re C_{11}$ component probes the asymmetry in the system; a non-zero value reveals the asymmetry.

In Fig. 9 we show results for the C_{00} and $\Re C_{11}$ components from the spherical decomposition of our ΛK^+ system in the 0-10% centrality bin (red circles). Results from a number of other components within the decomposition, as well as for our ΛK^0_S and ΛK^- systems, are contained in App. **??**. Along with the experimental data in Fig. 9, we have also included results from THERMINATOR simulation for an impact parameter of b = 2 fm (gold stars). As THERMINATOR does not include any final state effects, we assumed scattering parameters $(\Re f_0, \Im f_0, d_0)$ = (-1.16, 0.51, 1.08) and weighted the numerator pairs with $|\Psi|^2$, as discussed previously in Sec. **??** (with regard to Fig. **??**). Note, for the ΛK^+ system, THERMINATOR 2 predicts $\mu_{\text{out}} \approx 4$ fm, as shown in Fig. 10 As seen in the figures, the C_{00} signal is similar to that observed in our one-dimensional study. The $\Re C_{11}$ component shows a clear deviation from zero, and the negative value signifies that the Λ particles are, on average, emitted further out and/or earlier

than the K mesons (in defining our pairs, we take the heavier Λ as our first particle, which is opposite the normal convention). Therefore, as expected, our single particle Λ and K sources are separated in space-time.

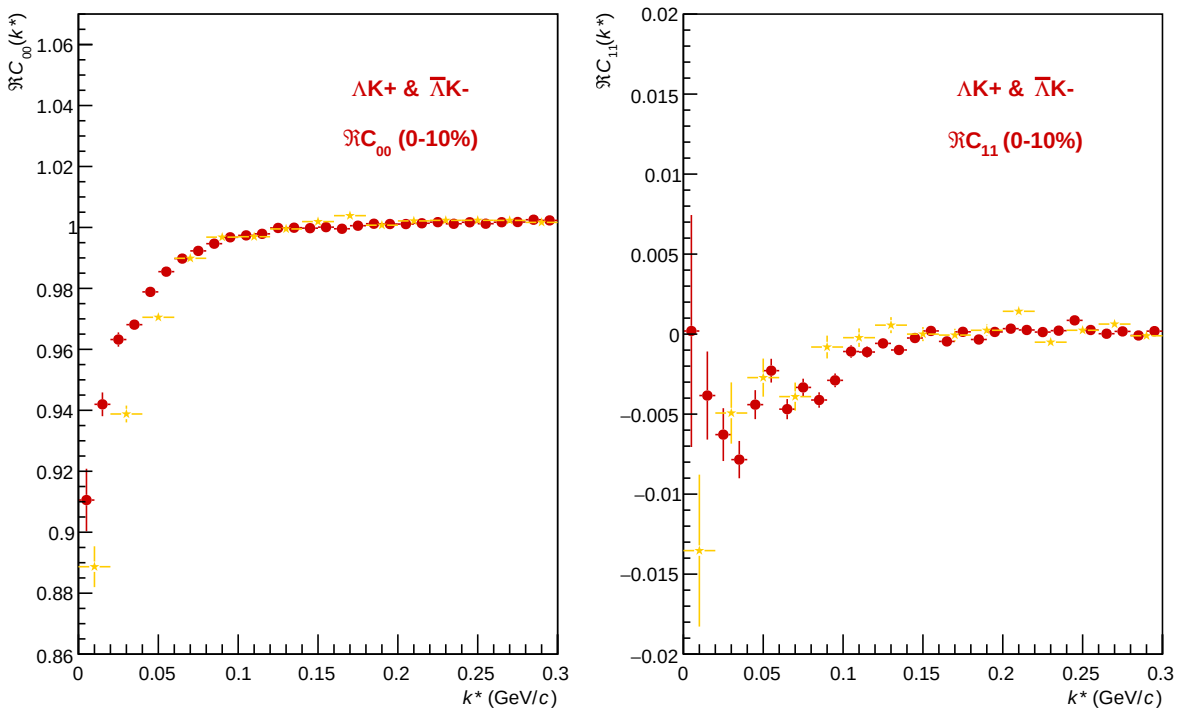

Fig. 9: C_{00} (left) and $\Re C_{11}$ (right) components of a spherical harmonic decomposition of the ΛK^+ correlation function for the 0-10% centrality bin. The C_{00} component is similar to the 1D correlation functions typically studied, and probes the overall size of the source. The $\Re C_{11}$ component probes the asymmetry in the system; a non-zero value reveals the asymmetry

Fig. 10 shows a closer look at the THERMINATOR simulation, whose spherical harmonic decomposition was shown along with the data in Fig. 9. The top left of Fig. 10a shows a fit to the one-dimensional correlation function from THERMINATOR. The scattering parameters are known precisely here, as they served as the weights used in the simulation, and are kept constant in the fit. We are interested at looking at the extracted one-dimensional source size here, so the λ parameter is also fixed at unity. The other three plots in Fig. 10a show the source distribution in the out (top right), side (bottom left), and long (bottom right) directions (all in the PRF). The source distributions have all been fitted with a Gaussian form, the result of which is printed within the respective plots. One immediately sees a significant shift in the out direction, $\mu_{\text{out}} \approx 4$ fm, and negligible shift in the other two directions, $\mu_{\text{side}} \approx \mu_{\text{long}} \approx 0$ fm. The figure demonstrates that, within the THERMINATOR model, the Λ is, on average, emitted further out that its K partner. Finally, Fig. 10b shows the distribution of the relative time of emittance, again in the PRF. The figure shows that the Λ is, on average, emitted earlier than its K partner. These two results from THERMINATOR 2 are as expected.

We end this section with a brief look at how a spatial separation of the single particle sources affects the radii extracted from a femtoscopic analysis. To achieve this, we use THERMINATOR in a similar fashion as described above, but with one important difference. Instead of taking the source information from THERMINATOR, we draw the source from pre-determined Gaussian distributions. In all cases, we take $R_{\text{out}} = R_{\text{side}} = R_{\text{long}} = 5$ fm, and $\mu_{\text{side}} = \mu_{\text{long}} = 0$ fm. Figure 11 shows an example of results

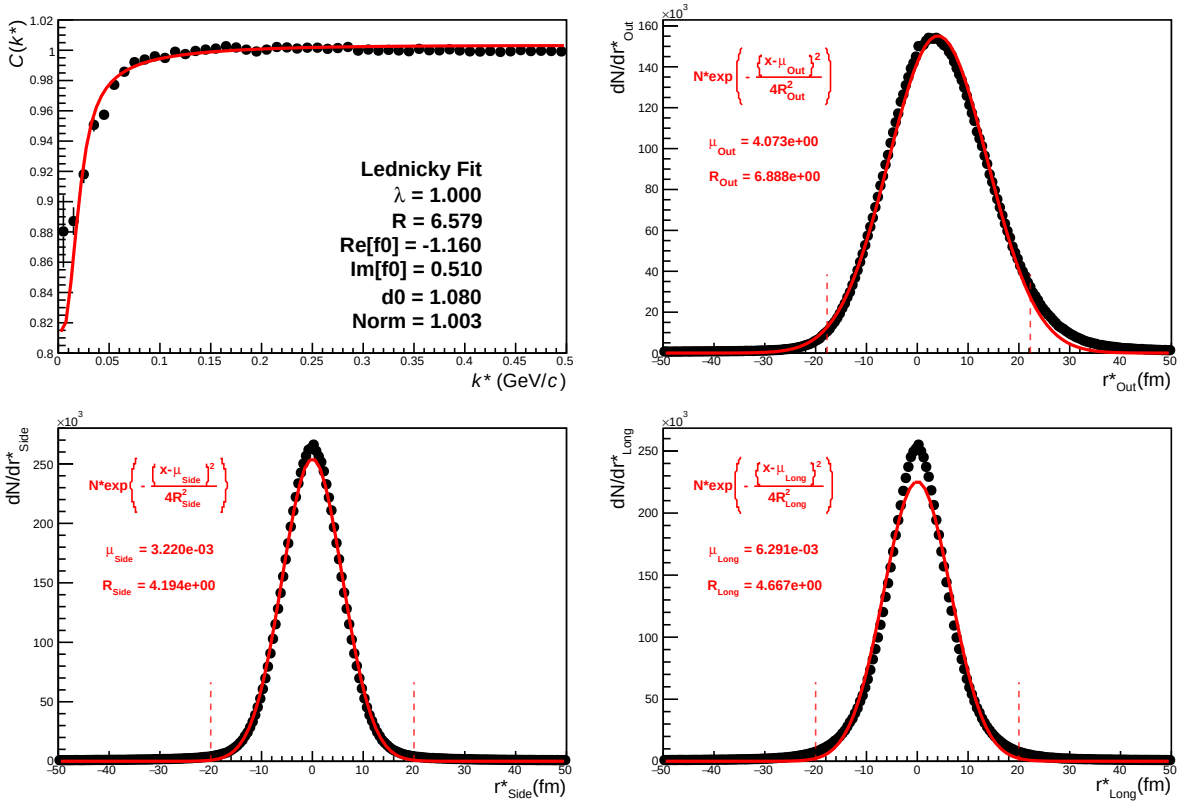

(a) (Top Left) Simple fit on simulation from THERMINATOR 2. Generated source in the (Top Right) out, (Bottom Left) side, and (Bottom Right) long directions.

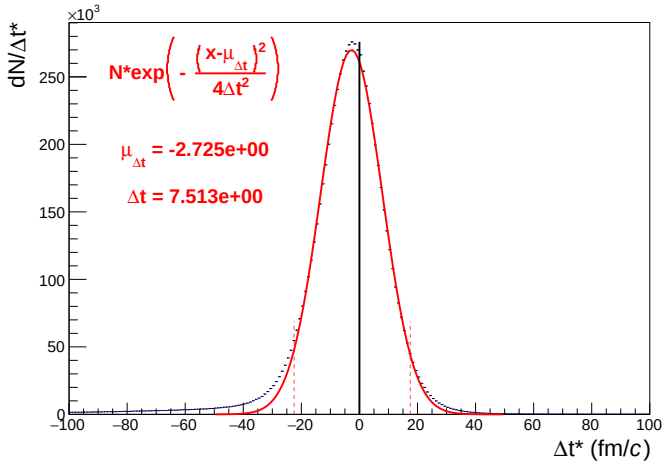

(b) Temporal characteristics of the source.

Fig. 10: Extracted radius when performing a simple fit on simulation from THERMINATOR 2, along with the spatio-temporal characteristics generated by the simulation.

obtained from THERMINATOR following this procedure, where $\mu_{\text{out}} = 3$ fm.

In Figure 12, we show results for the case of $\mu_{out} = 1$ fm, $\mu_{out} = 3$ fm, and $\mu_{out} = 6$ fm. In this figure, we do not show the side and long distributions, as they appear identical to those shown in Fig. 11. The figure demonstrates that as the separation μ_{out} increases, so do the extracted femtoscopic radii. This is exactly as expected, and in agreement with our qualitative assessment of the curves generated by our numerical Koonin-Pratt integrator described above.

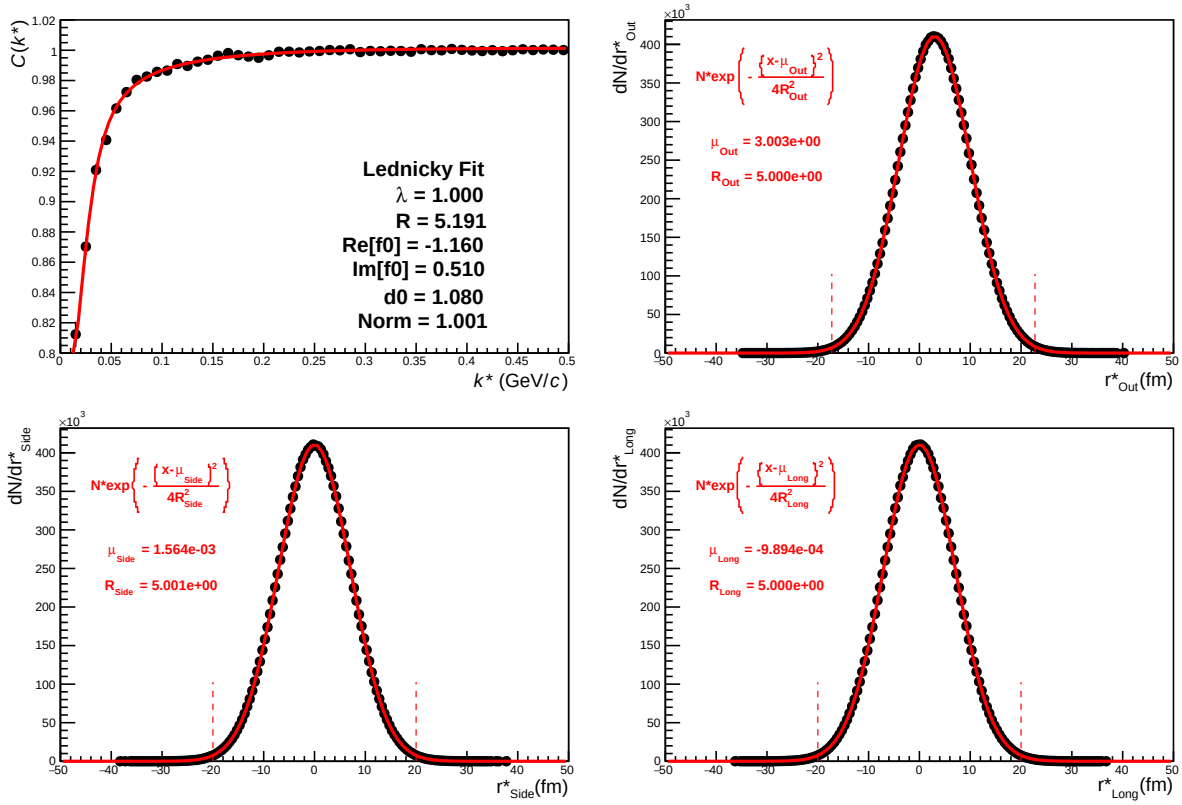

Fig. 11: THERMINATOR 2 simulation with artificial Gaussian source. The figure shows the extracted radius when performing a simple fit on simulation from THERMINATOR 2 (similar to Fig. 10a), except the space-time information provided by the simulation is ignored. Instead, the components of the spatial separation for each pair were drawn from Gaussian distributions, with $\sigma^2_{o,s,l} = 5$ fm, $\mu_{s,l} = 0$ fm, and $\mu_o = 3$ fm. The separation of emission in time was taken to be zero. (Top Left) Simple fit on simulation from THERMINATOR 2. Source in the (Top Right) out, (Bottom Left) side, and (Bottom Right) long directions.

Comparing non-identical to identical particle result

Non-identical femtoscopic analyses are not so simply compared to identical particle studies. However, a method was presented in which the single particle source sizes can be extracted using three related femtoscopic measurements, which can then be related to the results from identical particle studies [**?**]. Extracting the single particle source size from and identical study simply amounts to dividing the extracted radii by $\sqrt{2}$. For non-identical studies, the procedure is not so simple. As introduced in Sec. **??**, assuming the single particle sources are three dimensional Gaussians with offsets in the "out" direction, the pair source distribution is also a Gaussian with offset in the "out" direction. The form of the Gaussian is given in Eq. **??**, and reproduced here for convenience.

$$\begin{aligned} S_{AB}(\mathbf{r}) \propto \exp\left(-\frac{[r_{out} - (\mu_{a,out} - \mu_{b,out})]^2}{2(R^2_{a,out} + R^2_{b,out})}\right) \times \ldots \\ \times \exp\left(-\frac{r^2_{side}}{2(R^2_{a,side} + R^2_{b,side})}\right) \times \ldots \\ \times \exp\left(-\frac{r^2_{long}}{2(R^2_{a,long} + R^2_{b,long})}\right) \end{aligned} \tag{1}$$

which demonstrates $\mu_{ab,out} = \mu_{a,out} - \mu_{b,out}$, and $R^2_{ab,i} = R^2_{a,i} + R^2_{b,i}$. Unfortunately, with a single femtoscopic measurement, the two single particle source sizes cannot be extracted. However, in Ref. [**?**], the

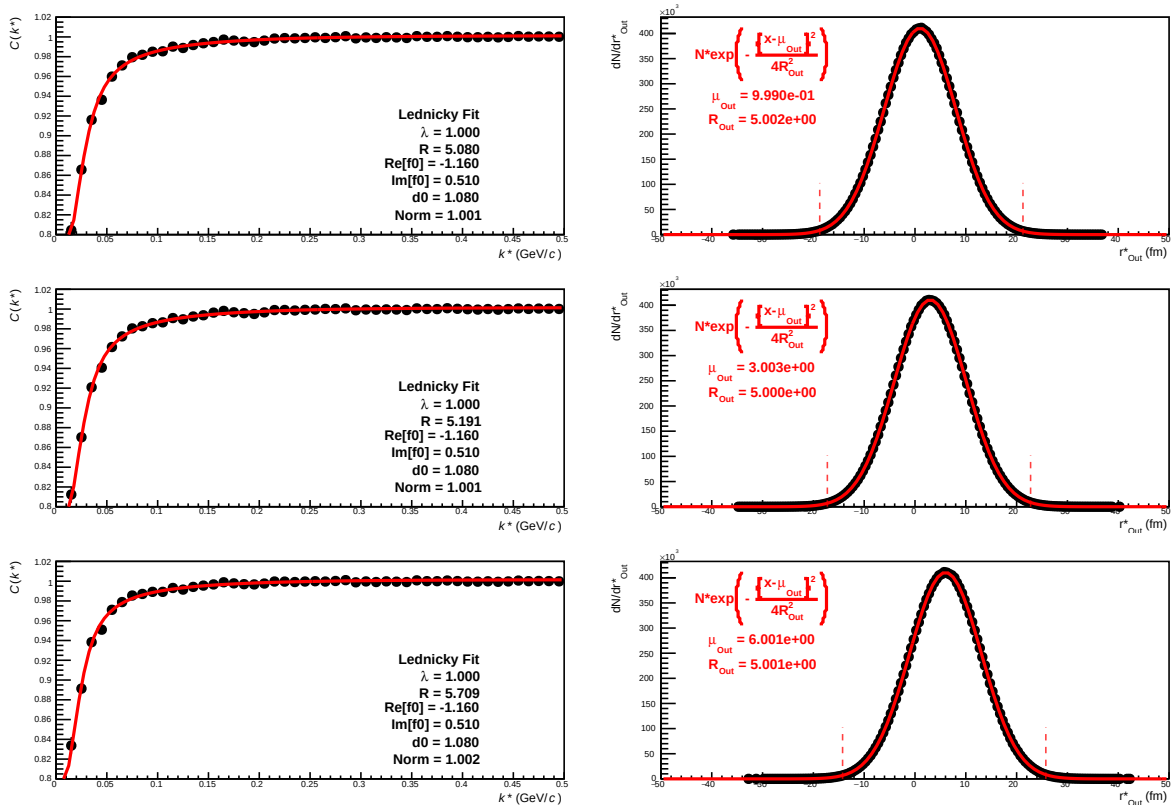

Fig. 12: Probing the effect of varying the source shift in the outward direction, μ_{Out}, within the THERMINATOR 2 framework. To achieve this, we formed particle pairs from the simulation, but altered their spatial characteristics by drawing the out, side, and long components from pre-determined Gaussian distributions. The plots on the left show fits resulting from the sources (in the out direction) shown on the right. The sources in the side and long directions are not shown, and are both Gaussians of width 5 fm centered at the origin for all cases. Moving from top to bottom, μ_{Out} increase from 0 to 6 fm, the effect of which clearly increases the effective radius extracted in the fit.

author demonstrated that using three related femtoscopic measurements, the single particle sizes can be extracted. However, this method does rely on including μ_{out} in the fit.

Performing measurements of the systems πK, πp and Kp permits one to extract the single particle π, K, and p source sizes. In Ref. [**?**], the author assumed $R_{\text{out}} = R_{\text{side}} = \sigma_f$, $R_{\text{long}} = 1.3\sigma_f$ and $\mu_{\text{side}} = \mu_{\text{long}} = 0$. Furthermore, having reliable estimates of the scattering parameters for the systems, only two fit parameters, R_{out} and μ_{out} were left, and easily extracted. Given the fact that $R^2_{ab,i} = R^2_{a,i} + R^2_{b,i}$, for the three systems we therefore have

$$\begin{aligned} \sigma_f^{\pi\text{K}} &= \sqrt{\sigma_f^{\pi 2} + \sigma_f^{\text{K}2}} \\ \sigma_f^{\pi\text{p}} &= \sqrt{\sigma_f^{\pi 2} + \sigma_f^{\text{p}2}} \\ \sigma_f^{\text{Kp}} &= \sqrt{\sigma_f^{\text{K}2} + \sigma_f^{\text{p}2}} \end{aligned} \tag{2}$$

These three equations can then be solved for the single particle source sizes

$$\begin{aligned}\sigma_f^{\pi} &= \sqrt{\left(\sigma_f^{\pi\mathrm{K}2} + \sigma_f^{\pi\mathrm{p}2} - \sigma_f^{\mathrm{Kp}2}\right)/2} \\ \sigma_f^{\mathrm{K}} &= \sqrt{\left(\sigma_f^{\pi\mathrm{K}2} - \sigma_f^{\pi\mathrm{p}2} + \sigma_f^{\mathrm{Kp}2}\right)/2} \\ \sigma_f^{\mathrm{p}} &= \sqrt{\left(-\sigma_f^{\pi\mathrm{K}2} + \sigma_f^{\pi\mathrm{p}2} + \sigma_f^{\mathrm{Kp}2}\right)/2}\end{aligned} \tag{3}$$

These extracted single particle source sizes can then be compared to those obtained using identical particle femtoscopy to check for consistency. Unfortunately, with our analysis, we are unable to include μ_{out} in our fit, and therefore are unable to utilize a similar type of solution.